technologies

Article

Behind the Door: Practical Parameterization of Propagation Parameters for IEEE 802.11ad Use Cases

Luciano Ahumada *,†, Erick Carreño †, Albert Anglès †, Diego Dujovne † and Pablo Palacios Játiva †

Escuela de Informática y Telecomunicaciones, Universidad Diego Portales, Santiago 8320000, Chile; erick.carreno@mail.udp.cl (E.C.); aangles1984@gmail.com (A.A.); diego.dujovne@mail.udp.cl (D.D.); pablo.palacios@mail.udp.cl (P.P.J.)

* Correspondence: luciano.ahumada@mail.udp.cl; Tel.: +56-9-9779-2920

† These authors contributed equally to this work.

Abstract: The integration of the 60 GHz band into the IEEE 802.11 standard has revolutionized indoor wireless services. However, this band presents unique challenges to indoor wireless communication infrastructure, originally designed to handle data traffic in residential and office environments. Estimating 60 GHz signal propagation in indoor settings is particularly complicated due to dynamic contextual factors, making it essential to ensure adequate coverage for all connected devices. Consequently, empirical channel modeling plays a pivotal role in understanding real-world behavior, which is characterized by a complex interplay of stationary and mobile elements. Given the highly directional nature of 60 GHz propagation, this study addresses a seemingly simple but important question: what is the impact of employing highly directive antennas when deviating from the line of sight? To address this question, we conducted an empirical measurement campaign of wireless channels within an office environment. Our assessment focused on power losses and distribution within an angular range while an indoor base station served indoor users, simulating the operation of an IEEE 802.11ad high-speed WLAN at 60 GHz. Additionally, we explored scenarios with and without pedestrian movement in the vicinity of wireless terminals. Our observations reveal the presence of significant antenna lobes even in obstructed links, indicating potential opportunities to use angular combiners or beamformers to enhance link availability and the data rate. This empirical study provides valuable information and channel parameters to simulate 60 GHz millimeter wave (mm-wave) links in indoor environments, paving the way for more efficient and robust wireless communication systems.

Keywords: indoor signal propagation; IEEE 802.11ad; mm-waves; wireless LAN

Citation: Ahumada, L.; Carreño, E.; Anglès, A.; Dujovne, D.; Palacios Játiva, P. Behind the Door: Practical Parameterization of Propagation Parameters for IEEE 802.11ad Use Cases. *Technologies* **2024**, *12*, 85. https://doi.org/10.3390/technologies12060085

Academic Editor: Sotirios K. Goudos

Received: 3 May 2024
Revised: 28 May 2024
Accepted: 5 June 2024
Published: 7 June 2024

1. Introduction

Nowadays, the integration of adaptive systems in millimeter band transceivers has become imperative to mitigate the substantial losses attributed to path loss [1,2]. However, the efficacy of using millimeter waves (mm-waves) for high-speed data transmission remains a subject of intense debate in current research [3], mainly due to the significant overhead associated with the implementation of beamforming and other complementary techniques. This challenge is further compounded by the emergence of shadowing effects induced by non-static and non-stationary scatterers, such as individuals in motion proximate to the antennas deployed at the base access point (AP) or to the user terminal (STA) [4].

The 60 GHz propagation channel exhibits clustered characteristics [4–8], where the received signal mainly comprises a direct beam and first-order reflected waves [5]. Consequently, an effective mitigation of path loss can be achieved through the installation of high-gain antennas that are precisely aligned at both ends of the wireless link. Alternatively,

pointing strategies, as described in [8], offer an interesting approach. Although these strategies increase the burden of coordination on the system, they also amplify losses induced by minor pointing errors.

Recent advances in wireless mm-wave propagation have explored various environmental configurations; however, these studies have largely overlooked the combined impact of pedestrians and non-line-of-sight (NLOS) links, which more accurately reflect real-world wireless channel conditions. In reference [9], the authors present large-scale path loss models and temporal statistics derived from indoor measurement campaigns conducted using rotating horn-type directional antennas operating at 28 GHz and 73 GHz frequencies. Although this study establishes a channel model for a stationary office environment close to APs and STAs, it does not address the effects of pedestrian obstruction, which can lead to intermittent signal disruptions over time. These disruptions pose a significant challenge, particularly considering the high transmission rates characteristic of such links, which often reach gigabits per second (Gbps). To bridge this gap, our research efforts involve measuring temporal and angular variations in received power with and without the presence of individuals near the antennas.

The authors in [6] describe a measurement experiment in a living room, also called indoor-to-indoor (I2I), over the 60 GHz channel using 20 dBi directional antennas at the same height. They investigated the impact of moving pedestrians in a setup composed of a single pedestrian traveling across the link over a small number of crossing locations and measured the data transmission loss. Their preliminary findings reveal that pedestrian movement generates a temporary reduction in signal-to-noise ratio (SNR) of more than 20 dB.

In the domain of indoor propagation, our study investigates the impact of positioning an STA behind a door when an AP is situated in a hallway. Specifically, we examine how this transition from LOS to NLOS affects signal strength and potential power loss.

Building on the investigation of indoor propagation challenges, previous studies have utilized ray-tracing simulations to assess channel characteristics [10]. For instance, reference [6] employed the knife-edge model to simulate pedestrian obstructions, while reference [5] presents a measurement-based spatio-temporal statistical channel model for short-range millimeter-wave links in large office rooms, malls, and station scenarios. These studies utilized ray-tracing techniques to account for first- and second-order reflections from various surfaces, inducing temporal channel fluctuations. The insights obtained from these investigations are invaluable for refining theoretical or simulation models. However, when considering duplicate fades, several assumptions are inherent. To enhance the accuracy of such simulations, our work contributes empirical channel parameters tailored to this specific context.

Reference [7] presents the dynamic characteristics of the 60 GHz radio propagation channel through measurements conducted in an open-space office environment. Measurements aim to quantify the impact of natural human movements on path loss both before and during work hours, allowing for a comparison between dynamic scenarios and static conditions when the office is devoid of occupants. Using a vector network analyzer (VNA) with a 2 GHz bandwidth, they recorded a total of 9900 power loss measurements over 11 h for each receiver position. Five receiver positions were strategically chosen to examine three types of scenarios: LOS, obstructed line-of-sight (OLOS), and NLOS. From the data collected, the authors derived the loss of the channel path (PL), its probability density function (PDF), and its cumulative distribution function (CDF). In comparison, our method enhances current techniques by calculating the signal loss generated by walls and doors in office environments for similar height directional antennas. Moreover, in our work, we include the impact of those working inside workplaces who are not blocking the connection (i.e., sitting, doing their regular work), changing the multipath pattern.

The authors in [11] provide an innovative on-air measurement setup for millimeter bands, explaining the derived parameters using a multi-probe anechoic chamber to emulate shadow fading generated by the human body. To examine the geometry of the paths, they

employed ray tracing and image processing techniques. They concluded that shadow fades were influenced by the link's architecture, as well as the interaction between the multipath pattern and pedestrian trajectories. Our results expand previous studies by providing actual data from a real-world setting (outside the anechoic chamber) in which pedestrians move along a predetermined or random route. This is important not only for comparing outcomes but also for calibrating theoretical/ray-tracing simulation models to enhance accuracy.

Based on the state of the art and existing comparisons and shortcomings, the goal of this work is to present an empirical measurement methodology and analyze the outcomes in both LOS and NLOS conditions, focusing on scenarios where an access point provides indoor stations compliant with the IEEE 802.11ad standard. The proposed empirical approach aims to determine the additional power required to mitigate channel losses, ensuring adequate coverage and availability for user stations. Furthermore, we offer insights into the angular distribution of received power at the tested locations, serving as supplementary data to enhance understanding of the underlying physical processes. Our study adds to the list of wireless channel estimation models, including theoretical, empirical, and simulation models. Although the existing literature predominantly presents statistics derived from empirical or simulated results, our research focuses on improving empirical models. By furnishing realistic data for mm-wave channel parameters, we enable the refinement of these models to align with empirical findings. Consequently, these adjusted parameters can be seamlessly integrated into both theoretical and simulation models.

The rest of the article is organized as follows: Section 2 describes the setup of the measurements performed in the scenarios. Section 3 presents the experimental methodology and work scenarios. Section 4 presents and discusses the experimental results obtained from our study and the study cases. Finally, Section 5 concludes the article by summarizing the key findings and recommend future work and improvements.

2. Measurement Setup

Measurements were performed using an experimental development kit operating in the 60 GHz band. This kit incorporates Vubiq transmitter and receiver stations (model V60WGD03) [12]. In our measurements, a continuous wave (CW) signal is transmitted in the first channel of the IEEE 802.11ad standard (58.32 GHz), generated from an external input signal. The latter corresponds to an unmodulated tone at 70 MHz, injected from a Rohde & Schwarz signal generator (SMC100A).

As illustrated in [13], a CW method is commonly used to measure transmission losses. It is based on transmitting a sine wave signal at a fixed frequency using a narrow frequency filter at the receiver. We used a high-power transmission setting and a low-noise amplifier in the receiver to obtain a very high sensitivity. Typical hardware solutions are relatively compact and simple, allowing extensive signal strength sampling in large areas quickly and conveniently. However, the main disadvantage of this approach is that the contribution of each of the multipath behaviors of the transmitted signal cannot be identified. The CW measurement illustrates what an actual commercial equipment receives. For example, the measurement can represent the power level received by a sub-carrier of an OFDM system, as defined in IEEE 802.11ad networks. Therefore, our results are valid for analyzing the performance of wireless stations at indoor locations, and the observed changes in received power for each angle reproduce what commercial equipment would observe in a typical use case.

Our measurement methodology is currently widely used to model the parameters of wireless channels [14–16]. However, the main advantage of our approach is that the actual received power can be observed with the configuration of a typical commercial product, for a range of frequency bands, using rotary directive antennas.

At both link ends, we use directive horn-type 24 dBi antennas with a 12° half-power beamwidth (HPBW). The transmitter gain and the receiver gain (excluding antenna gains) are 26 dB and 49 dB, respectively. The effective isotropically radiated power (EIRP) is set

at 35 dBm in all the cases under test, and the noise floor of the system is −54 dBm. Since the IEEE 802.11ad standard employs OFDM transceivers [8], our narrowband approach is useful to evaluate the performance of the system from the per-carrier perspective.

To measure the angular distribution of power in the receiving unit, we used a microcontroller based on a rotary arm to define the angle sequence and synchronize the measurement period. This measurement scheme allowed separate power samples to be obtained every 1.8°. We acquired 1000 power samples for each arm position, which were recorded with a USB power meter connected to the Vubiq board output and a personal computer. The power resolution of the USB meter is less than 1 dB, and its noise floor is −60 dBm.

To verify the stability of the equipment, we also performed a calibration measurement process in a stationary environment with a link length of 2 m. We observed negligible resulting temporal fluctuations, with variations below 1 dB in all cases. As expected, these shallow fades were well described by a Rician distribution with large calibration K-factors, greater than 30 dB. A summary of the technical parameters used for the measurement campaign is shown in Table 1.

Table 1. Summary of the experimental setup and parameters.

Parameter	Description and Value
Mm-wave band development kit	Vubiq V60WGD03 (AP/STA), Vubiq Networks Incorporated, Irvine, CA, USA
Operating frequency	58.32 GHz
Signal generator	Rohde & Schwarz SMC100A, Rohde & Schwarz GmbH & Co KG, Munich, Germany
Baseband input signal	Unmodulated continuous wave at 70 MHz
Antennas	Horn type, 24 dBi Gain, 12° HPBW
AP gain	26 dB
STA gain	49 dB
EIRP	35 dBm
System noise floor	−54 dBm
USB power meter resolution	<1 dB
USB power meter noise floor	−60 dBm
Angular distribution system	Arduino-controlled Rotary arm
Angular resolution	1.8°
Number of samples per angular position	1000
Calibration condition	Stationary environment
Calibration link length	2 m
Calibration fluctuation	<1 dB
Calibration fading distribution	Rician with K-factor > 30 dB

3. Experimental Methodology

We conducted the measurements within the Faculty of Engineering and Sciences at the Universidad Diego Portales (UDP) in Santiago, Chile. The tested area (Figures 1–3) is an open floor with offices separated by internal partition walls and plaster. In this sense, NLOS-tested links will cross these particleboard interior divisions, and the propagation path (when blocked) will only be obstructed by this material. Note that building materials such as walls and furniture, among others, affect the results. Metallic (iron, steel, copper) desks and chairs will probably create more multipath than wood. Obstacle sizes and shapes will also alter the channel, especially at high-frequency bands like the mm-wave band. Therefore, our results will contribute to the literature by providing empirical data on a use case that has received little attention, being useful to simulate the channel without making assumptions about the angular distribution and power losses.

Figure 1. Measurement location of AP and STA in Pos. 5.

Figure 2. Measurement location of STA "hiding" inside office B.

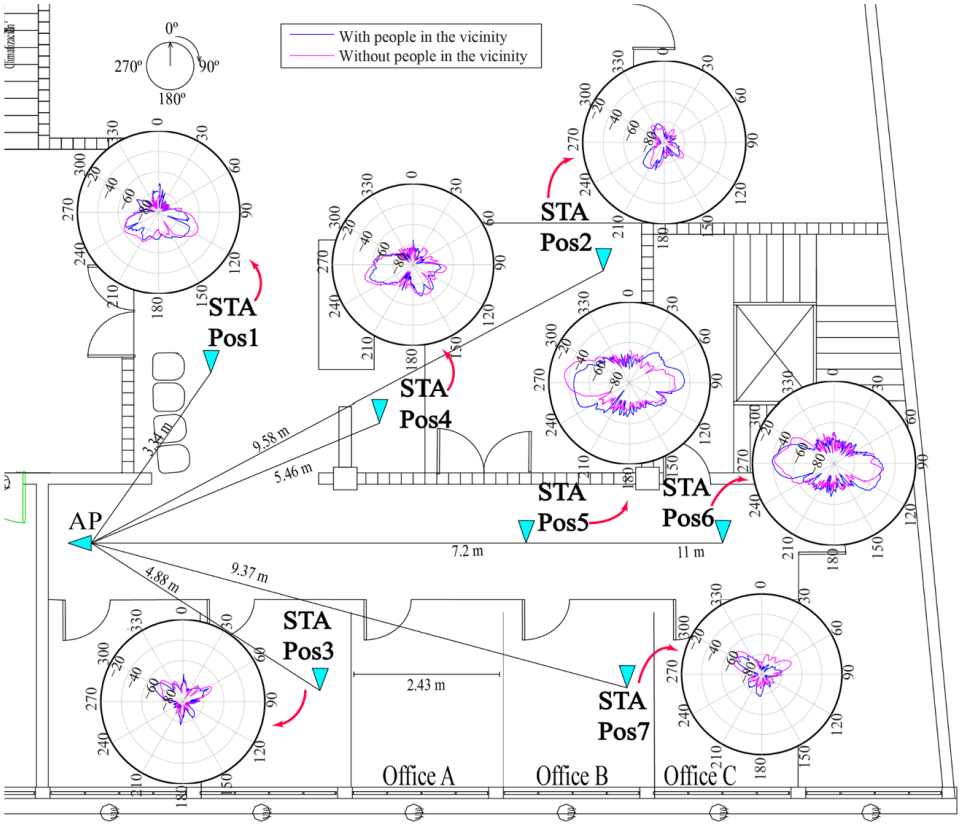

Figure 3. Diagram of locations and angular profiles of received power (dBm unit) in the STA antenna terminals.

The exterior wall of the building is made of reinforced concrete, a standard setting that complies with current seismic building regulations. As shown in Figure 3, the horn antennas at the AP and STA are depicted with a blue triangle. A red arrow relates the polar graph with the STA position tested. Note that we used the following convention for polar coordinates in all the results: 0° points to the top of Figure 3. In each polar diagram, the maximum power received at the terminals of the STA antenna is −20 dBm, and the minimum is −100 dBm, with 20 dB per division. Finally, the magenta lines represent the case where there are no people in the vicinity of the STA (the case of 'empty room'), while the blue lines show the case where seven people circulate in the area.

We designed three representative use cases. The first one describes the distribution of the received power concerning the angle for different LOS/NLOS STA positions. Given that our objective is to model losses caused by physical obstructions (distinct from losses caused by pedestrians), this case is considered a static condition (i.e., without people circulating in the area). The second case replicates the first scenario but includes people inside the offices (one person per office, seated, doing their usual work). For the first two cases, the AP is placed at one end of the corridor, with a fixed orientation toward the other end (see Figures 1 and 2). The STA was placed in seven different locations, as shown in Figure 2. The antennas' height was set at 1.25 m.

The third and final case measures power losses in an indoor propagation scenario: The access point is positioned in a corridor, and the STA is located behind a door (i.e., we move the STA slightly away from the LOS, as in Figure 2, transitioning from LOS to NLOS). We used six new measurement locations to compute these losses, as described in the following section.

4. Experimental Results

In this section, we present and discuss the experimental results obtained from our study. Our proposed goals were thoroughly analyzed in three different cases, providing us with conclusive evidence of their characteristics.

4.1. Case 1: Angle Power Distribution in a Static Scenario

In this case, where no movement exists, we measured the power distribution with the angle for each location, as detailed in the Experimental Methodology Section. Figure 2 presents a polar diagram of the STA antenna's power received (in dBm) for each measured location. In the figure, we observe that the geometric direction of the LOS does not always lead to the highest power level; consequently, we calculate the angle between the LOS direction and the direction of maximum received power for each case.

Table 2 shows this estimate, where θ_{TX} is defined as the angle of the shortest path to the AP (i.e., LOS). In turn, θ_{MaxPR} corresponds to the angular direction for the maximum received power for each position. Δ_{PR} represents the difference in dB between the powers received at θ_{MaxPR} and θ_{TX}, and $\Delta_\theta = \theta_{MaxPR} - \theta_{TX}$ represents the angular difference between them. In this way, if the maximum power is received from the LOS, Δ_{PR} and Δ_θ will be close to 0. Both antennas (AP and STA) are adjusted to 0° in the elevation plane. The results in Table 2 quantify the benefits of using electronic antenna pointing schemes in the azimuth plane as the best transmission strategy. From the results, we infer that these eventual benefits are not negligible, particularly in NLOS links: Δ_{PR} is up to 13 dB in Pos. 2 (without people), where the largest possible power can be obtained by pointing towards the office entrance. As expected, in positions where the link includes the LOS (Pos. 5 and 6), the dominant beam comes from a direction close to the LOS. Note that mm-wave channels are usually conceived as the LOS. Most of the published simulation results assume that the radiation pattern of highly directive antennas filters the multipath contribution, only considering the LOS. We observed (as evaluated in [17]) that this is not the case. Work in [17] shows that the mm-wave channel is clustered. Then, a single pedestrian moving along the path or near the antenna may block the contribution of significant clusters, turning θ into a random variable.

It is worth noting that, under conditions of total stability (no movement of people in the vicinity of the AP or STA), the link is stable, showing a peak-to-peak variation of no more than 0.15 dB.

Table 2. Difference table between $\theta_{TX}(^\circ)$ and $\theta_{MaxPR}(^\circ)$. NP represents the case without people and P the case with people.

Position	$\theta_{TX}(^\circ)$	$\theta_{MaxPR}(^\circ)$		Δ_{PR} (dB)		$\Delta_{\theta}(^\circ)$	
		NP	P	NP	P	NP	P
Pos 1. (NLOS)	220	117	245	11	13	103	25
Pos 2. (NLOS)	245	219	227	13	8	26	18
Pos 3. (NLOS)	290	315	299	8	6	25	9
Pos 4. (NLOS)	256	254	257	0.6	0.5	2	1
Pos 5. (LOS)	270	274	266	0.9	0	4	4
Pos 6. (LOS)	270	273	272	0.6	0.5	3	2
Pos 7. (NLOS)	280	312	293	11	16	32	13

The received power can reduce the SNR to 0 dB, or be equal to the noise floor if there is no beamforming or adaptive pointing techniques applied to the receiving unit. On the other hand, the use of omnidirectional antennas does not take advantage of the different lobes appearing for each polar diagram depicted in Figure 3. Since there are at least two lobes with significant power in the positions under test, it is feasible to use diversity schemes or angular combiners to take advantage of a multipath increasing SNR.

4.2. Case 2: Power Distribution with an Angle in the Presence of People in the Vicinity of the STA

In this case, six pedestrians move freely and randomly (similar to the works [4,7]) in the vicinity of the transmitter and receiver. They are 20- to 23-year-old male students, with 1.70–1.75 m heights. Thus, it is reasonable to think that this traffic may generate variable shadowing over time. We present the results in Figures 4 and 5. In these figures, we observe the standard deviation of the received power as a function of the angle for the positions in Figure 3. The average received power per angle is shown in the polar diagrams of the figure mentioned above in the blue data series.

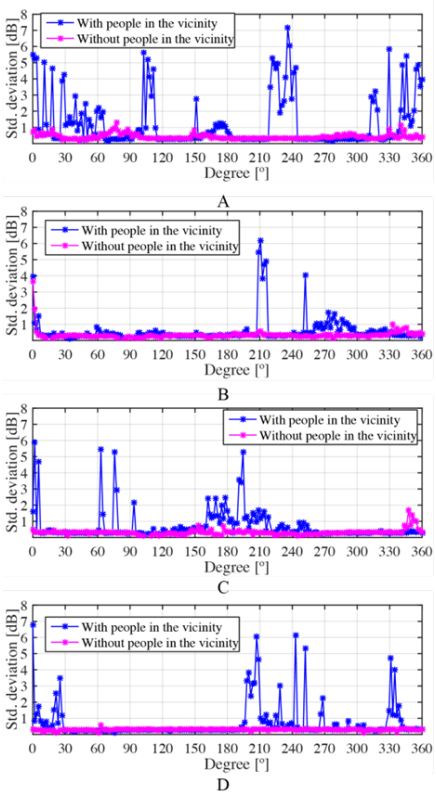

Figure 4. Standard deviation of positions 1–4: (**A**) Pos. 1 (NLOS), (**B**) Pos. 2 (NLOS), (**C**) Pos. 3 (NLOS), and (**D**) Pos. 4 (NLOS).

The largest fluctuations recorded were 6–7 dB, more frequent in NLOS links. This differs significantly from Case 1, where the angular distribution of the standard deviation did not exceed 1 dB (magenta series). Although the power fluctuations produced by the movement of the person seated inside the offices could be considerable, this does not occur uniformly for all angles. In general, we observed that the largest standard deviation was recorded at angles close to θ_{TX}. Their position, as well as the dominant directions and secondary lobes, is coherent with the results in Case 1.

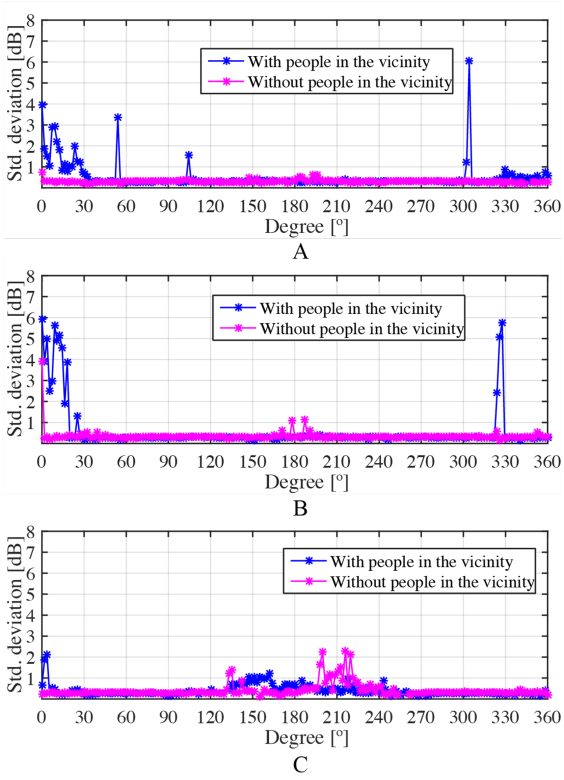

Figure 5. Standard deviation of positions 5–7: (**A**) Pos. 5 (LOS), (**B**) Pos. 6 (LOS), and (**C**) Pos. 7 (NLOS).

4.3. Case 3: Penalties for Locating the STA behind a Door

In the third case under study, we evaluate the losses obtained by "hiding" the STA inside offices A, B, and C (see Figure 6). Measurements in this case are made without the presence of people on the entire floor. Figure 6 shows the angular power profiles obtained in the STA for the six positions under test: three positions where the STA is in the corridor (blue line) and three where the STA is inside the offices (magenta line). From the former configurations, we can deduce that, in LOS positions, the dominant lobe comes from the direction of the AP (270°), revealing a secondary lobe arriving from the end of the corridor (90°). By moving the STA away from the LOS, the maximum power entering the office is recorded near 0° (i.e., towards the corridor). The losses observed when "hiding" the STA are significant in relation to what is measured in the LOS: 35, 38, and 26 dB for offices A, B, and C, respectively, when comparing the maximums measured in each case.

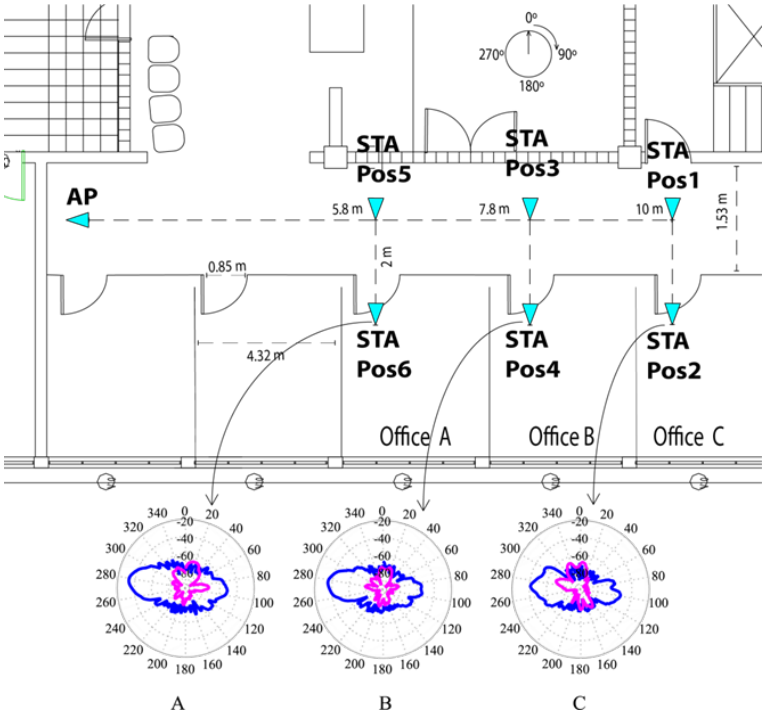

Figure 6. Positions tested to estimate the losses after "hiding" from the LOS with corresponding angular profiles of received power (dBm unit) in the STA for the LOS (blue) and NLOS cases (magenta): (**A**) Pos. A, (**B**) Pos. B, and (**C**) Pos. C.

5. Conclusions and Future Work

Empirical results are always contingent on the geometry, measurement setup, and system configuration. That is why all empirical campaigns contribute to the literature by computing channel parameters in different scenarios. Specifically, in this work, we discuss several fundamental propagation parameters computed from empirical data in a typical and relevant use case of IEEE 802.11ad networks that has only been partially covered in the literature. These parameters are relevant for tuning simulators or calibrating computational analyses of wireless networks by incorporating physical layer impairments. This allows the design of cross-layer evaluations, testing the performance of upper-layer protocols for a non-ideal physical layer.

As a further contribution, this article presents empirical results for the design of IEEE 802.11ad networks: an indoor high-speed wireless local area network operating at 60 GHz. We have demonstrated that, with the angular distribution of the received power, the link is stable, and there is more than one useful lobe if no significant movement exists along the link. Although moving pedestrians can cause substantial power losses, there are still a significant number of lobes to combine in angular combiners (MRC, SC, EGC) or in a beamformer to enhance link performance. We also note that small pointing errors can bring the STA to the noise floor. Moreover, we did not observe significant changes in the angular profiles of the received power at the STA when people worked at their desks (inside offices, moving freely, without walking). For the tested scenario, "hiding" the STA antenna behind a door (when transmitting from the aisle) showed significant losses (up to 40 dB) even if the link length did not change significantly.

Regarding future work, we intend to extend these results to the outdoor–indoor case, where an outdoor base station provides service to indoor users. This will be representative of the operation of fifth-generation cellular systems, where the 60 GHz band is fundamental for high-speed data transmissions under very low latency constraints.

Author Contributions: Conceptualization, L.A., E.C. and A.A.; methodology, L.A., E.C. and A.A.; software, L.A., E.C. and A.A.; validation, L.A., E.C. and A.A.; formal analysis, L.A., E.C. and A.A.;

investigation, L.A., E.C. and A.A.; resources, L.A., E.C. and A.A.; data curation, L.A., E.C. and A.A.; writing—original draft preparation, L.A., E.C. and A.A.; writing—review and editing, D.D. and P.P.J.; visualization, L.A., E.C. and A.A.; supervision, L.A.; project administration, L.A.; funding acquisition, L.A. All authors have read and agreed to the published version of the manuscript.

Funding: This work was partially supported by ANID through the grant Fondecyt/Postdoc 3140045, and it was also partially funded by the Proyecto Conicyt/Basal Advanced Center for Electrical and Electronic Engineering (AC3E, Proyecto Basal FB0008), ANID FONDECYT Iniciación 11240799, ANID FONDECYT Regular 1211132, and SENESCYT "Convocatoria abierta 2014-primera fase (Acta CIBAE-023-2014)".

Institutional Review Board Statement: Not applicable

Informed Consent Statement: Not applicable

Data Availability Statement: The raw data supporting the conclusions of this article will be made available by the authors on request.

Acknowledgments: The authors would also like to express their gratitude to the CYTED AgIoT Project (520rt0011) and the CORFO CoTH2O Consortium for their generous support.

Conflicts of Interest: The authors declare no conflicts of interest.

References

1. Alkhateeb, A.; El Ayach, O.; Leus, G.; Heath, R.W. Channel estimation and hybrid precoding for millimeter wave cellular systems. *IEEE J. Sel. Top. Signal Process.* **2014**, *8*, 831–846. [CrossRef]
2. Tezergil, B.; Onur, E. Wireless backhaul in 5G and beyond: Issues, challenges and opportunities. *IEEE Commun. Surv. Tutor.* **2022**, *24*, 2579–2632. [CrossRef]
3. Dilli, R. Performance analysis of multi user massive MIMO hybrid beamforming systems at millimeter wave frequency bands. *Wirel. Netw.* **2021**, *27*, 1925–1939. [CrossRef]
4. Sharmin, S.; Boby, S.M.; Mahmud Boby, S. Characterization of WLAN System for 60 GHz Residential Indoor Environment Based on Statistical Channel Modeling. *Int. J. Wirel. Microw. Technol.* **2020**, *10*, 42–58. [CrossRef]
5. Haneda, K.; Järveläinen, J.; Karttunen, A.; Kyrö, M.; Putkonen, J. A statistical spatio-temporal radio channel model for large indoor environments at 60 and 70 GHz. *IEEE Trans. Antennas Propag.* **2015**, *63*, 2694–2704. [CrossRef]
6. Jacob, M.; Priebe, S.; Kürner, T.; Peter, M.; Wisotzki, M.; Felbecker, R.; Keusgen, W. Extension and validation of the IEEE 802.11 ad 60 GHz human blockage model. In Proceedings of the 2013 7th European Conference on Antennas and Propagation (EuCAP), Gothenburg, Sweden, 8–12 April 2013; IEEE: Piscataway, NJ, USA, 2013; pp. 2806–2810.
7. El Hajj, M.; Zaharia, G.; El Zein, G.; Farhal, H.; Sadek, S. Measurements of a dynamic 60 ghz radio channel in an open-space office. In Proceedings of the 2020 14th European Conference on Antennas and Propagation (EuCAP), Copenhagen, Denmark, 15–20 March 2020; IEEE: Piscataway, NJ, USA, 2020; pp. 1–5.
8. Nitsche, T.; Cordeiro, C.; Flores, A.B.; Knightly, E.W.; Perahia, E.; Widmer, J.C. IEEE 802.11 ad: Directional 60 GHz communication for multi-Gigabit-per-second Wi-Fi. *IEEE Commun. Mag.* **2014**, *52*, 132–141. [CrossRef]
9. Maccartney, G.R.; Rappaport, T.S.; Sun, S.; Deng, S. Indoor office wideband millimeter-wave propagation measurements and channel models at 28 and 73 GHz for ultra-dense 5G wireless networks. *IEEE Access* **2015**, *3*, 2388–2424. [CrossRef]
10. Játiva, P.P.; Azurdia-Meza, C.A.; Sánchez, I.; Seguel, F.; Zabala-Blanco, D.; Firoozabadi, A.D.; Gutiérrez, C.A.; Soto, I. A VLC channel model for underground mining environments with scattering and shadowing. *IEEE Access* **2020**, *8*, 185445–185464. [CrossRef]
11. Fierro, L.A.; Maggi, E.C.; Vazquez, A.A.; Schkolnik, D. Empirical results for human-induced shadowing events for indoor 60 GHz wireless links. *IEEE Access* **2020**, *8*, 44522–44533. [CrossRef]
12. Anglès-Vázquez, A.; Carreno, E.; Ahumada, L.S. Modeling the effect of pedestrian traffic in 60-GHz wireless links. *IEEE Antennas Wirel. Propag. Lett.* **2017**, *16*, 1927–1931. [CrossRef]
13. Zaidi, A.; Athley, F.; Medbo, J.; Gustavsson, U.; Durisi, G.; Chen, X. *5G Physical Layer: Principles, Models and Technology Components*; Academic Press: Cambridge, MA, USA, 2018.
14. Oladimeji, T.T.; Kumar, P.; Oyie, N.O. Propagation path loss prediction modelling in enclosed environments for 5G networks: A review. *Heliyon* **2022**, *8*, e11581. [CrossRef] [PubMed]
15. Al-Samman, A.M.; Azmi, M.H.; Al-Gumaei, Y.A.; Al-Hadhrami, T.; Abd. Rahman, T.; Fazea, Y.; Al-Mqdashi, A. Millimeter wave propagation measurements and characteristics for 5G system. *Appl. Sci.* **2020**, *10*, 335. [CrossRef]

16. Shaibu, F.E.; Onwuka, E.N.; Salawu, N.; Oyewobi, S.S.; Djouani, K.; Abu-Mahfouz, A.M. Performance of path loss models over mid-band and high-band channels for 5G communication networks: A review. *Future Internet* **2023**, *15*, 362. [CrossRef]
17. Maltsev, A.; Maslennikov, R.; Sevastyanov, A.; Khoryaev, A.; Lomayev, A. Experimental investigations of 60 GHz WLAN systems in office environment. *IEEE J. Sel. Areas Commun.* **2009**, *27*, 1488–1499. [CrossRef]